

Crustal thickness variations across the northern Tien Shan from teleseismic receiver functions

Hedwig A. Bump and Anne F. Sheehan

Cooperative Institute for Research in the Environmental Sciences (CIRES) and Department of Geological Sciences
University of Colorado at Boulder

Abstract. Variations in crustal thickness from the Kazakh Shield to the north-central Tien Shan are determined by receiver function analysis of broadband teleseismic P waveforms recorded on the Kyrgyzstan Seismic Telemetry Network (KNET). The receiver functions are calculated using a time-domain deconvolution approach, and are interpreted in terms of a single crustal layer, with thickness determined by a grid-search comparison of observed receiver functions with synthetics. Crustal thicknesses average 42 km in the southern Kazakh Shield and increase to approximately 60 km in the Tien Shan. Together with mass balance calculations, these results are consistent with the hypothesis that the compensation of the central Tien Shan relative to the Kazakh Shield are accommodated by an Airy-type crustal root, with a modest (300 kg/m^3) density contrast across the Moho.

Introduction

The Tien Shan fold belt system of Central Asia is one of the most tectonically active mountain ranges in the world, despite the fact that it is relatively far (approximately 1,500 km) from the active Indo-Eurasian collision zone. Present rates of deformation within the Tien Shan are anomalously high for intercontinental regions, leading to numerous studies attempting to explain the causes of deformation [e.g., *Tapponnier and Molnar, 1979; Lukk et al., 1995; Abdrakhmatov et al., 1996*].

Fault plane solutions determined by *Ni [1978]* and *Nelson et al. [1987]* indicate that thrust faulting on moderately dipping (35° - 55°) E-W trending faults predominates in the Tien Shan. Earthquakes on the southern edge of the Tien Shan and the Fergana Basin have fairly shallow depths (10-20 km), while those on the faults to the north of the Tien Shan can approach depths of 40 km or more. The deformation suggested by these earthquakes is in the form of N-S shortening, with the formation of basement uplifts flanked by moderately dipping thrust faults. *Burov et al. [1990]* find that Bouguer gravity anomalies over the Tien Shan are large and negative, and the western and central Tien Shan are isostatically compensated. Bouguer anomalies east of approximately 78.5°E indicate an uncompensated mass deficit, which *Burov et al. [1990]* predict is supported by thickened mantle lithosphere beneath the eastern Tien Shan.

Previous crustal models of the Tien Shan include large-scale averages of crustal structure with average crustal thickness of 50 - 55 km from both refraction [*Belousov et al., 1992*], and surface waves [*Cotton and Avouac, 1994*]. *Kosarev et al. [1993]* examined teleseismic receiver functions from a network of 14

intermediate period seismometers in the central and western Tien Shan. They find large differences in crustal velocities E and W of the Talasso-Fergana fault (TFF) with lower crustal velocities and a broad transitional Moho to the east, with crustal thickness of 55-60 km. They suggest that crustal shortening is the dominant mechanism controlling topography west of the TFF and that a mass deficit in the upper mantle contributes to the formation and support of the high elevations east of the fault. Seismic tomography work using both P and S waves from local and teleseismic events was performed using short period stations in the central and western Tien Shan [*Roecker et al., 1993*]. They also find that crust and upper mantle velocities E of the TFF are lower than those W of the fault. They find no evidence for a lithospheric root, and instead suggest that low velocities in the upper mantle imply the presence of a positive buoyancy force uplifting the mountains. They argue that an anomalously buoyant and presumably warm upper mantle makes the Tien Shan easier to deform than the surrounding lithosphere. P-SV conversions from the 410-km discontinuity are found to be 2 s earlier beneath the Tien Shan than beneath the Kazakh Shield [*Chen et al., 1997*], suggesting cool material near 410 km depth beneath the Tien Shan.

Our study area is bounded to the west by the TFF and extends to 75.5°E . While the previous work outlined above has provided a large scale view of structural variations along the Tien Shan mountain chain (trending east-west), we take advantage of a dense regional network in the central Tien Shan in order to

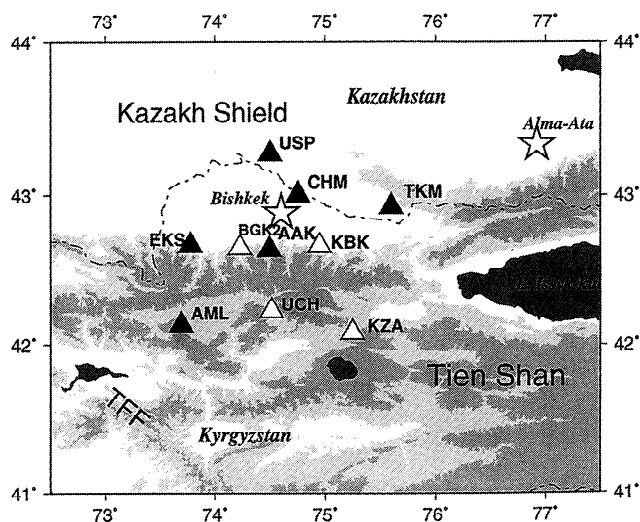


Figure 1. Location of KNET within Central Asia. Filled triangles are stations used in this study, open triangles are excluded from analysis. Elevations over 3000 m are shaded dark gray; 2000-3000 m, light gray. Stars mark large cities.

Copyright 1998 by the American Geophysical Union.

Paper number 98GL00516.
0094-8534/98/98GL-00516\$05.00

provide a detailed look at the north-south transition in crustal structure from the Kazakh Shield to the central Tien Shan, and its implications for the dynamics of the Tien Shan.

Data

The seismograms used in this study come from the Krygyz Seismic Network (KNET) in the north-central Tien Shan (Figure 1) [Vernon, 1992]. The network was originally composed of ten stations each with a three-component Streckeisen STS-2 broadband seismometer. The network lies in the north-central Tien Shan, along the boundary between the mountains and the Kazakh Shield to the north. From south to north, the stations KZA, AML, and UCH lie along the Kyrgyz Ridge between elevations of 3400 m to 3850 m; the stations AAK, KBK, BGK, and EKS lie along the northern foothills of the Tien Shan from 1360 to 1700 m; and the remaining three stations TKM, CHM, and USP lie along the southern rim of the Kazakh platform at elevations less than 1000 m (Table 1, Figure 1). Problems of telemetry are most common for the three mountain stations, AML, UCH and KZA, due to the remoteness of the stations. Usable seismic records from these stations, therefore, are fewer than for the other stations; sufficient data for this study were not obtained from stations KZA, UCH, or BGK.

The data used for this study include events recorded by the Kyrgyz Seismic Network between October 1991 and August 1994. For this study, teleseismic events between distances of 30° and 90° , $m_b \geq 6.0$, and good signal-to-noise ratio were selected. The resultant dataset consists of forty-two events largely from the western Pacific. The events are binned into seven subsets, each within a range of 16° in backazimuth. Selection criteria for records at each station was further restricted to those for which a minimum of three traces displayed coherence within the backazimuthal bin, and at least three backazimuth bins available.

Methods and Results

Receiver Functions

Several investigators have shown that the wavetrain of the teleseismic P arrival can be interpreted in terms of reflections and transmissions of mode-converted waves at discrete boundaries beneath the recording station [e.g., Owens *et al.*, 1984]. These techniques regard the recorded signal as a convolution of a source-time function, an instrument response, and a velocity structure, or "receiver" function. The primary underlying assumption of the receiver function technique is that compared to the direct arrival, *P*-to-*S* conversions from discontinuities beneath the receiver are much weaker on the vertical component

seismogram $v(t)$ than on the radial component $r(t)$. Therefore, $v(t)$ can be used as an estimate of the *P* source function incident at the base of the crust along with *P* reverberations, and *P*-to-*S* conversions are isolated by the deconvolution of $v(t)$ from $r(t)$.

We employ a time domain deconvolution approach for the determination of teleseismic receiver functions. In this approach, the convolutional relationship between the vertical and radial components of one or more seismograms is treated as an invertible system of time-domain equations for parameters of the receiver function. Thus, rather than stacking many individual receiver functions, we invert for a single receiver function from a suite of seismograms recorded at a given station. Further details on this technique can be found in Sheehan *et al.* [1995]. Frequency domain receiver functions were also constructed and compared with the time domain receiver functions, with similar results.

Radial receiver functions are estimated using the time domain techniques for each backazimuth. Synthetic receiver functions for a suite of plausible crustal thicknesses are sequentially tested to find the crustal thickness which gives the minimum root mean square difference between the observed receiver function and the corresponding synthetic. These synthetic receiver functions are generated using a plane layered model, with the thickness of the crustal layer differing incrementally for each calculation. This grid search technique allows visualization of the tradeoffs inherent in receiver function inversions in order to select the best model. Details of the trade-offs between various parameters using this technique are given in Sheehan *et al.* [1995].

The receiver functions are interpreted in terms of a single layer crust in order to determine gross crustal thickness variations across the north central Tien Shan. The main feature modeled is the first *P*-to-*S* conversion at the base of the crust (*Ps*). A constant crustal *P* wave velocity of 6.3 km/s was assumed, *S* wave velocity was obtained assuming a V_p/V_s ratio of 1.8, and crustal density from a Birch's law relation. Constants used for V_p and V_p/V_s are estimated from the 1D velocity models of Roecker *et al.* [1993]. Recent tomographic images of Ghose *et al.* [1998] show lateral variations in the mid and upper crustal structure beneath the northern Tien Shan, with regions of higher elevation underlain by lower velocity materials compared to the low-lying foreland to the north. The resolution of their models is poor at lower-crustal depths. On average, the mid-crustal velocity beneath the foreland is approximately 6.3 km/s, and beneath the mountains, 6.0 km/s. If consistent throughout the crust this lateral velocity variation will reduce our crustal thickness estimate for the mountains relative to the shield by approximately 2 km. Large lateral V_p/V_s variations are not observed [Ghose *et al.*, 1998], and sensitivity tests show that for reasonable variations in V_p/V_s crustal thickness estimates change by less than 2 km [Sheehan *et al.*, 1995].

We experimented with variously filtering the receiver functions and found that the Moho *Ps* phase shows greatest coherence across the array at periods greater than 2.5 s. At these low frequencies, complexities of scattering and other unmodeled phenomena are reduced, simplifying the data and making them more consistent from event to event. We therefore lowpass filter both data and synthetic receiver functions at 2.5 s before running the grid search. A shallow *P* to *S* conversion, presumably from the base of a sedimentary basin, is observed at several stations. To avoid complications due to sedimentary basin conversions, basin thickness was estimated using the timing of the basin *P*-to-*S* conversion as observed on unfiltered receiver functions, and the resulting sedimentary layer was included in the calculation of the

Table 1. Crustal Parameters.

Station	Lat. °N	Long. °E	Elev. m	Basin depth km	Crustal thick. km	s.d. km	Moho depth km
USP	43.27	74.49	740	3	42	1.6	41.3
CHM	42.99	74.75	655	4	37	4.2	36.3
TKM	42.86	75.31	960	3	44	2.9	43.0
EKS	42.66	73.78	1360	2	45	1.3	43.6
AAK	42.63	74.49	1680	2	51	6.5	49.3
AML	42.08	73.69	3400	0	60	1.4	56.6

Parameters used: *P* velocity of crust, 6.3 km/s; *S* velocity of crust, 3.5 km/s; density of crust 2800 kg/m³; *P* mantle, 8.0 km/s; *S* mantle, 4.4 km/s; density of mantle, 3300 kg/m³; *P* sediments, 4.5 km/s; *S* sediments, 2.6 km/s; sediment density, 2300 kg/m³. s.d. = standard deviation.

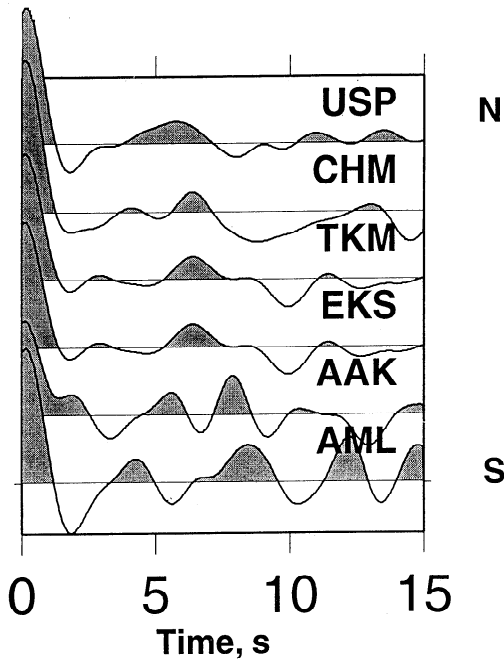


Figure 2. Receiver functions for 66°- 82° backazimuth bin. Stations ordered by latitude with northernmost station (USP) at top. Each receiver function shown is determined from 3 to 5 events using time domain inversion deconvolution technique which jointly inverts for a single receiver function from several input seismograms.

synthetics (Table 1). Velocity for the sedimentary layer is estimated from Kosarev *et al.* [1993].

For each station, a receiver function is obtained for each backazimuthal set for which a minimum of three coherent events has been recorded (e.g., Figure 2). The full backazimuth range sampled is from 30°- 150° and backazimuth bins range from 5°- 16° in width. By examining receiver functions for a single station from several events within a small range of backazimuths and event-to-station distances, the noise level is reduced, and deterministic structure of the crust is more easily identified. Furthermore, lateral crustal variations such as dipping planar interfaces can be more easily interpreted from azimuthal trends in the receiver functions. The grid search is run, and the crustal thickness value which produces the smallest RMS residual between the observed and synthetic receiver function is tabulated (Figure 3a,b). A crustal thickness is determined for each azimuthal bin, and these crustal thickness values are averaged to obtain a final crustal thickness for a station. Variations in depth with backazimuth are minimal for stations USP (Figure 3b), CHM, TKM, EKS, and AML. Large variations in crustal depth with backazimuth are found at station KBK, with thinner crust systematically from SE azimuth stations, and multiple minima in inversions from E and NE azimuth stations, making interpretation of structure beneath this station in terms of a single flat layer inappropriate. Some variation with backazimuth is observed at station AAK through all but one backazimuth inversions have a global minima within 5 km of the median of 52.5.

Variance within the dataset for each station is interpreted as actual complexity of the crustal structure, and is used as an estimate of the uncertainty in the crustal thickness values (Table 1). The largest variations with backazimuth are observed at station AAK. The crustal thickness values calculated range from 37 to 60 km across the KNET array (Table 1). In general, the crustal thickness values increase from north to south across the

network, with increasing station elevation. As described earlier, lateral velocity variations in the region [Ghose *et al.*, 1998] likely moderate this crustal thickness difference by 2 km.

Test of Airy Root

The Airy root hypothesis can be tested by a simple examination of the relationship between observed elevation and Moho depth. For a region supported by Airy isostasy, the mean Moho depth (z_m) should vary linearly with the mean elevation (ϵ) at each station through the equation $z_m = (\rho_t / \Delta\rho_m)\epsilon + z_{mREF}$, where ρ_t is the density of the topography (crust above sea level), $\Delta\rho_m$ is the density contrast across the Moho, and z_{mREF} is the crustal thickness of a section at sea level. Mean elevation is determined by averaging topography around the measurement point using a function describing the flexure of a plate from a point load [Jones *et al.*, 1996]. In our case, the elastic thickness of the plate is assumed to be 25 km, based on previous studies of the

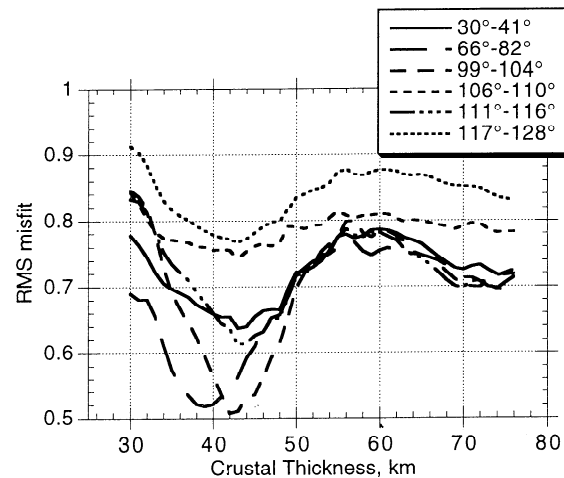
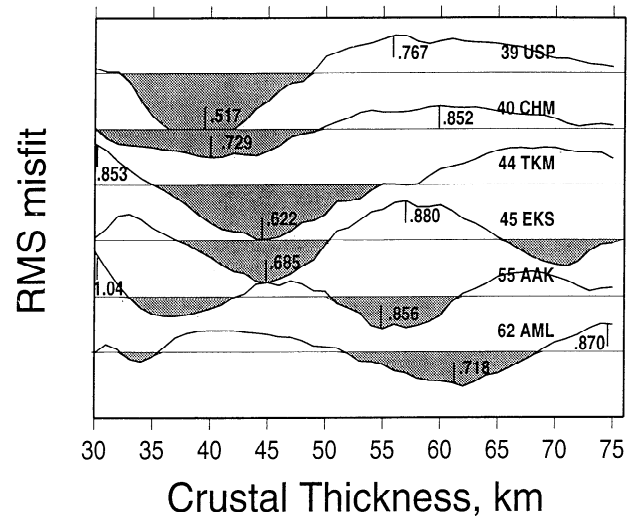


Figure 3. (a) Examples of root-mean-square (RMS) misfit between observed and synthetic receiver functions at KNET stations calculated for a suite of crustal thicknesses for 66° - 82° backazimuth. Numbers represent crustal thickness determined from this particular backazimuth inversion. Values of highest and lowest data normalized RMS residual given on each trace. (b) RMS misfit versus crustal thickness for inversion from six different backazimuths at station USP. Backazimuth range used in each inversion shown in legend. The patterns of the RMS curves are broadly similar for each backazimuth, with minima near 42 km.

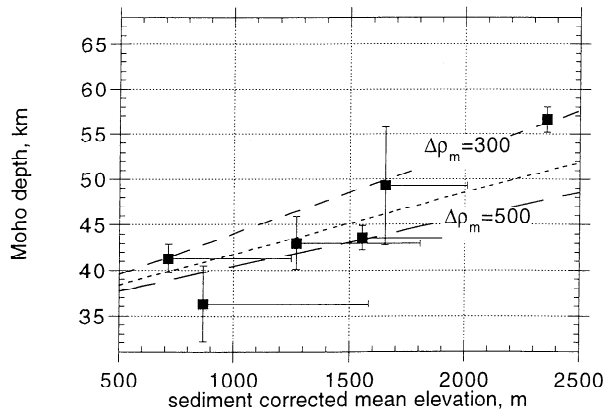


Figure 4. Moho depth versus sediment-corrected mean station elevation. Lines relating average elevation and Moho depth are shown for $z_{mREF} = 35$ km, $\rho_t = 2700$ kg/m³, and $\Delta\rho_m$ in 100 kg/m³ increments from 300 to 500 kg/m³, from top to bottom. Weighted linear fit to data has correlation coefficient $R = 0.923$, $z_{mREF} = 31.3 \pm 2.1$ km and $\Delta\rho_m = 272 \pm 34$ kg/m³ (assuming $\rho_t = 2700$ kg/m³). Horizontal bar indicates position of data point with sediment effects neglected.

region [Burov *et al.*, 1990], and the resulting integration is over a disk of radius approximately 250 km. The elevation is then corrected for presence of sediments by reducing the elevation an amount equal to the compaction necessary to make the sediments have the same density as the crust. Lines relating average elevation and Moho depth are shown for $z_{mREF} = 35$ km, $\rho_t = 2700$ kg/m³, and $\Delta\rho_m$ as indicated in Figure 4. A least squares line fit to the data shown (mean elevation and Moho depth) has correlation coefficient $R = 0.923$ and results in values of $z_{mREF} = 31 \pm 2$ km, $\rho_t = 2700$ kg/m³ (fixed), and $\Delta\rho_m = 272 \pm 34$ kg/m³. Global estimates of $\Delta\rho_m$ are typically around 500 kg/m³ [e.g., Bullen, 1975; Dziewonski and Anderson, 1981], though a recent study indicates that values on the order of 300 kg/m³ are more appropriate for continental regions [Martinec, 1994]. Thus, the value of $\Delta\rho_m$ that we obtain is somewhat lower than the typical value of 500 kg/m³ assumed in studies of this type, indicating that the density contrast at the Moho might be slightly less than in other regions. The presence of a small density contrast across the Moho concurs with the Kosarev *et al.* [1993] model. Values for these parameters were also determined using actual station elevation rather than mean elevation, and mean elevation determined using an elastic plate thickness of 5 km. Using these elevations, the range in z_{mREF} and $\Delta\rho_m$ is found to be 36.8 - 40.1 km and 468 - 613 kg/m³, respectively, giving us a qualitative feel for the uncertainties in our z_{mREF} and $\Delta\rho_m$ estimates. Eliminating the sediment correction results in a lower value of $\Delta\rho_m$ (Figure 4). While there is some scatter, in all cases the linear fit to the data is good, indicating that a simple Airy root with a constant $\Delta\rho_m$ is consistent with our data.

Conclusions

The main results of this paper are summarized in Table 1. The crustal thicknesses that we find from receiver function analysis range from 37 km in the Kazakh Shield to 60 km in the north central Tien Shan. We observe that in general the crust thickens with increasing elevation. Thus our results are consistent with a simple model of crustal shortening across the Tien Shan, with a relatively low density contrast at the Moho allowing for the presence of low density upper mantle.

Acknowledgments. We thank F. Vernon for setup and maintenance of the KNET array, and the JSPC at the University of Colorado, Boulder, for data management and discussions on the project; in particular, we

thank M. Ritzwoller, D. Harvey, and A. Levshin. R. Mellors provided the maps for Figure 1, and Figures 1-3a were drafted with GMT software [Wessel and Smith, 1991]. We thank R. Mellors, J. Cassidy, and an anonymous reviewer for helpful reviews. This work was supported in part by funding from a Grant-in-Aid of Research from the University of Colorado Council on Research and Creative Work.

References

- Abdrakhmatov, K. Ye., S. A. Aldazhanov, B. H. Hager, M. W. Hamburger, T. A. Herring, K. B. Kalabaev, V. I. Makarov, P. Molnar, S. V. Panasyuk, M. T. Prilepin, R. E. Reilinger, I. S. Sadybakasov, B. J. Souter, Yu. A. Trapeznikov, V. Ye. Tsurkov, and A. V. Zubovich, Relatively recent construction of the Tien Shan inferred from GPS measurements of present-day crustal deformation rates, *Nature*, **384**, 450-453, 1996.
- Belousov, V. V., N. I. Pavlenkova, and G. N. Kvyatkovskaya, Structure of the crust and upper mantle in the [former] USSR, *International Geology Review*, **34**, 279-297, 1992.
- Bullen, K. E., *The Earth's Density*, Chapman and Hall, London, 1975.
- Burov, E. V., M. G. Kogan, H. Lyon-Caen, and P. Molnar, Gravity anomalies, the deep structure, and dynamic processes beneath the Tien Shan, *Earth Planet. Sci. Lett.*, **96**, 367-383, 1990.
- Chen, Y. H., S. W. Roecker, and G. L. Kosarev, Elevation of the 410 km discontinuity beneath the central Tien Shan: Evidence for a detached lithospheric root, *Geophys. Res. Lett.*, **24**, 1531-1534, 1997.
- Cotton, F., and J. P. Avouac, Crust and upper mantle structure under the Tien Shan from surface-wave dispersion, *Phys. Earth Planet. Int.*, **84**, 95-109, 1994.
- Dziewonski, A. M., and D. L. Anderson, Preliminary Reference Earth Model, *Phys. Earth Planet. Int.*, **25**, 297-356, 1981.
- Ghose, S., M. W. Hamburger, and J. Virieux, Three-dimensional velocity structure and earthquake locations beneath the northern Tien Shan of Kyrgyzstan, central Asia, *J. Geophys. Res.*, *in press*, 1998.
- Jones, C. H., J. R. Unruh, and L. J. Sonder, The role of gravitational potential energy in active deformation in the southwestern United States, *Nature*, **381**, 37-41, 1996.
- Kosarev, G. L., N. V. Petersen, L. P. Vinnik, and S. W. Roecker, Receiver functions for the Tien Shan analog broadband network: Contrasts in the evolution of structures across the Talasso-Fergana fault, *J. Geophys. Res.*, **98**, 4437-4448, 1993.
- Lukk, A. A., S. L. Yunga, V. I. Shevchenko, and M. W. Hamburger, Earthquake focal mechanisms, deformation state, and seismotectonics of the Pamir-Tien Shan region, Central Asia, *J. Geophys. Res.*, **100**, 20,321-20,343, 1995.
- Martinec, Z., The density contrast at the Mohorovicic discontinuity, *Geophys. J. Int.*, **117**, 539-544, 1994.
- Nelson, M. R., R. McCaffrey, and P. Molnar, Source parameters for 11 earthquakes in the Tien Shan, Central Asia, determined by P and SH waveform inversion, *J. Geophys. Res.*, **92** (B12), 12,629-12,648, 1987.
- Ni, J., Contemporary tectonics in the Tien Shan region, *Earth Planet. Sci. Lett.*, **41**, 347-354, 1978.
- Owens, T. J., G. Zandt, and S. R. Taylor, Seismic evidence for an ancient rift beneath the Cumberland Plateau, Tennessee: A detailed analysis of broadband teleseismic P waveforms, *J. Geophys. Res.*, **89**, 7783-7795, 1984.
- Roecker, S. W., T. M. Sabitova, L. P. Vinnik, Y. A. Burmakov, M. I., Golvanov, R. Mamatkanova, and L. Munirova, Three-dimensional elastic wave velocity structure of the western and central Tien Shan, *J. Geophys. Res.*, **98**, 15,779-15,795, 1993.
- Sheehan, A. F., G. A. Abers, C. H. Jones, and A. L. Lerner-Lam, Crustal thickness variations across the Colorado Rocky Mountains from teleseismic receiver functions, *J. Geophys. Res.*, **100**, 20391-20404, 1995.
- Tapponnier, P., and P. Molnar, Active faulting and Cenozoic tectonics of the Tien Shan, Mongolia and Baykal regions, *J. Geophys. Res.*, **84**, 3425-3459, 1979.
- Vernon, F., Kyrgyzstan Seismic Telemetry Network, *IRIS Newsletter*, **7-9**, XI, 1, 1992.
- Wessel, P., and W. H. F. Smith, Frc software helps map and display data, *Eos Trans. Amer. Geophys. Union*, **72**, pp. 441, 445-446, 1991.

Anne F. Sheehan, Department of Geological Sciences, Campus Box 399, University of Colorado, Boulder, Colorado 80309-0216 (email: afs@mantle.colorado.edu)

(Received: August 5, 1996; Revised: January 26, 1998; Accepted: January 30, 1998)